PAPER

Structural and thermoelectrical characterization of epitaxial Sb$_2$Te$_3$ high quality thin films grown by thermal evaporation

To cite this article: Georg Bendt *et al* 2018 *Semicond. Sci. Technol.* **33** 105002

View the article online for updates and enhancements.

IOP ebooks™

Bringing you innovative digital publishing with leading voices to create your essential collection of books in STEM research.

Start exploring the collection - download the first chapter of every title for free.

Structural and thermoelectrical characterization of epitaxial Sb₂Te₃ high quality thin films grown by thermal evaporation

**Georg Bendt[1], Kevin Kaiser[1], Alla Heckel[1], Felix Rieger[2], Dennis Oing[3],
Axel Lorke[3], Nicolas Perez Rodriguez[4], Gabi Schierning[4],
Christian Jooss[2] and Stephan Schulz[1,5]** (iD)

[1] Faculty of Chemistry, Inorganic Chemistry, and Center for Nanointegration Duisburg-Essen (CENIDE),
University of Duisburg-Essen, Universitätsstr. 7, D-45114 Essen, Germany
[2] Institute of Material Physics, University of Göttingen, D-37077 Göttingen, Germany
[3] Faculty of Physics and Center for Nanointegration Duisburg-Essen (CENIDE), University of Duisburg-
Essen, Lotharstraße 1, D-47048 Duisburg, Germany
[4] Institute for Metallic Materials, Leibniz Institute for Solid State and Materials Research Dresden (IFW
Dresden), Helmholtzstr. 20, D-01069 Dresden, Germany

E-mail: stephan.schulz@uni-due.de

Abstract
Thermal evaporation of Sb₂Te₃ powder was systematically studied under various pressure and
temperature conditions. Low pressure experiments ($5 \cdot 10^{-6}$ mbar) conducted inside a horizontal
tube reactor at a temperature range of 500 °C–600 °C generated rough polycrystalline films on
Si(100) substrates. Based on these experiments, the chemical composition of the resulting films
were determined by the furnace temperature. Enhancing the reactor pressure to 20 mbar shifted
the growth zone towards higher temperature ranges and yielded highly *c*-oriented Sb₂Te₃ films
on Si(100) and Al₂O₃(0001) substrates. Additional experiments were conducted inside a special
reactor containing two independent heaters to study the effects of the evaporator and substrate
temperatures independently. In contrast to the samples generated in the previous reactor, a two-
zone heating reactor allowed the growth of epitaxial Sb₂Te₃ films with a very smooth surface
topology on Al₂O₃(0001) substrates, as shown by SEM, EDX, XPS, and HRTEM. The electrical
in-plane conductivity of the Sb₂Te₃ films decreased with increasing temperature, ultimately
reaching 3950 S $\cdot$ cm^{-1} at 300 K. The films showed a *p*-type carrier concentration of
$4.3 \cdot 10^{-19}$ cm^{-3} at 300 K and a very high carrier mobility of 558 cm$^2 \cdot$ V$^{-1} \cdot$ s^{-1}. The Seebeck
coefficient increased monotonically from 94 μV $\cdot$ K^{-1} at 270 K to 127 μV $\cdot$ K^{-1} at 420 K.

Supplementary material for this article is available online

Keywords: PVD, Sb₂Te₃, epitaxy, thermoelectricity, thin film

(Some figures may appear in colour only in the online journal)

1. Introduction

Since the early studies of Werner Haken in 1910, binary
tedradymite-type materials such as Sb₂Te₃ and Bi₂Te₃ remain

amongst the most studied thermoelectric materials until today [1]. These binary materials as well as their solid ternary solutions $(Sb_xBi_{1-x})_2Te_3$ show excellent thermoelectric performance near room temperature ($<300\,°C$) [2]. On the other hand, topological insulators are a class of materials that exhibit an insulating bulk state and a topologically protected metallic surface state with a Dirac-like band structure [3–8]. Interestingly, high-quality *c*-oriented epitaxial Sb_2Te_3 thin films have been extensively investigated over the last decade due to their promising potential to serve as thermoelectric or topological insulating materials in various fields of technical applications. Despite the growing interest for these materials, complex anisotropic crystal structures (space group $R\bar{3}m$ (#166)) often favor the formation of rough surface morphologies, thus hampering the formation of high-quality epitaxial films. In addition, high deposition temperatures which are generally required to achieve a high surface mobility of the adatoms typically give Te deficient materials. Consequently, Te lattice sites are replaced by Sb anti-site defects, which ultimately influences the electronic properties of the resulting film.

Several deposition techniques including physical and chemical deposition methods were applied in the growth of epitaxial tetradymite-type thin films. However, a more detailed analysis demonstrated that *metal organic chemical vapor deposition* (MOCVD) and *molecular beam epitaxy* (MBE) are the only processes suitable for the deposition of highly stoichiometric epitaxial tetradymite films with very smooth surface areas [9–11]. Unfortunately, both deposition techniques demand high requirements on the experimental setup and vacuum conditions. Long deposition times, relatively small-sized substrates (MBE), toxicity and air/moisture sensitivity of the likely used metal organic precursors (MOCVD) are additional drawbacks. In contrast, *physical vapor deposition* (PVD) in which purified material powders are evaporated and subsequently deposited on a given substrate, proved to be a better alternative for thin film deposition. Due to the simplicity and industrial scalability of PVD, several authors have investigated the deposition of Sb_2Te_3 films either by thermal co-evaporation of elemental Sb and Te powders or by thermal evaporation of Sb_2Te_3 powder. In fact, PVD processes were also applied for the growth of ternary solid solutions such as $(Bi_xSb_{1-x})_2Te_3$ and $Bi_2(Te_xSe_{1-x})_3$ [12–15]. Goncalves *et al* reported on the growth of polycrystalline Sb_2Te_3 films on polyimide and glass substrates at substrate temperatures ranging from $150\,°C$–$200\,°C$; the resulting films showed high Seebeck coefficients of up to 190 $\mu V \cdot K^{-1}$ [16]. The same group later reported on the growth of *n*-type Bi_2Te_3 films on glass, silicon, and polyimide substrates by thermal co-evaporation of Bi and Te powder at a low pressure of $5 \cdot 10^{-6}$ mbar [17]. Lin *et al* have successfully grown Sb_2Te_3 films on SiO_2 substrates at low substrate temperatures ($T_{Sub} = 50\,°C$–$150\,°C$) which showed a Seebeck coefficient of up to 112 $\mu V \cdot K^{-1}$ and a power factor of 3.94 $\mu V \cdot cm^{-1} \cdot K^{-2}$ [18, 19]. However, the films were found to contain elemental tellurium of which the concentration was strongly dependent of the substrate temperature; the tellurium concentration decreased with increasing temperature.

The thermal (co-)evaporation of tedradymite films is usually performed under high vacuum conditions, while the resulting films are typically grown at low substrate temperatures ($T < 200\,°C$). Unfortunately, the resulting films are often amorphous or nanocrystalline, and can exhibit high electrical resistivity which make an additional annealing step necessary. It is noteworthy that high substrate temperatures are beneficial for the quality of the film. For example, Zou *et al* have grown Sb_2Te_3 films by thermal co-evaporation on glass substrates at 150, 230 and 260 °C substrate temperatures. Films deposited at $T_{Sub} = 260\,°C$ showed the highest Seebeck coefficient (165 $\mu V \cdot K^{-1}$) and a low electrical resistivity of 1.14 $m\Omega \cdot cm$ [20]. Comparable findings were reported by Huang *et al* for Sb_2Te_3 films which were grown by co-evaporation methods on SiO_2 substrates at a substrate temperature of 230 °C and a working pressure of 10^{-6} mbar. The films showed a high degree order on *c*-orientation, but displayed a very rough surface morphology due to the formation of freestanding Sb_2Te_3 hexagons [21].

To the best of our knowledge, the growth of epitaxial tetradymite-type material films with a smooth and homogeneous substrate morphology has not been reported to date. Herein however, we report on the growth of high-quality Sb_2Te_3 films by thermal evaporation of Sb_2Te_3 powder and systematic investigations on the influence of the deposition parameters including pressure conditions, evaporation and deposition temperature, substrate material and reactor design. In addition, the transport properties of epitaxial Sb_2Te_3 films were determined.

2. Experimental section

General. Sb_2Te_3 (99.999%) powder was commercially available (abcr) and used as received. Si(100) and Al_2O_3(0001) substrates were obtained from Crystec.

Reactor I. Initial experiments were carried out in a horizontal quartz tube reactor (figure 1) at a working pressure of $5 \cdot 10^{-6}$ mbar and evaporation/deposition time of 30 min. The temperature of the furnace was raised to the evaporation temperature ($T_{evap} = 500\,°C$–$600\,°C$) and halted for 1 h. Upon reaching isothermal conditions, the powder sample holder (molybdenum boat) containing Sb_2Te_3 powder was magnetically transferred to the center of the furnace. Si(100) substrates (10 mm $\cdot$ 50 mm) were placed next to the Sb_2Te_3 powder in the temperature gradient at the tube outlet. After 30 min of film deposition, the system furnace was cooled to ambient temperature within 30 min under vacuum.

Reactor II. Sb_2Te_3 thin films were grown within 15 min on Al_2O_3(0001) substrates in a vertical reactor (figure 1) at a 20 mbar reactor pressure, which was established by a membrane pump. The Sb_2Te_3 powder and the substrate were heated independently. The evaporator temperature was varied from 540 °C–620 °C and the substrate temperature was varied from 300 °C–400 °C. After 15 min of film deposition, the
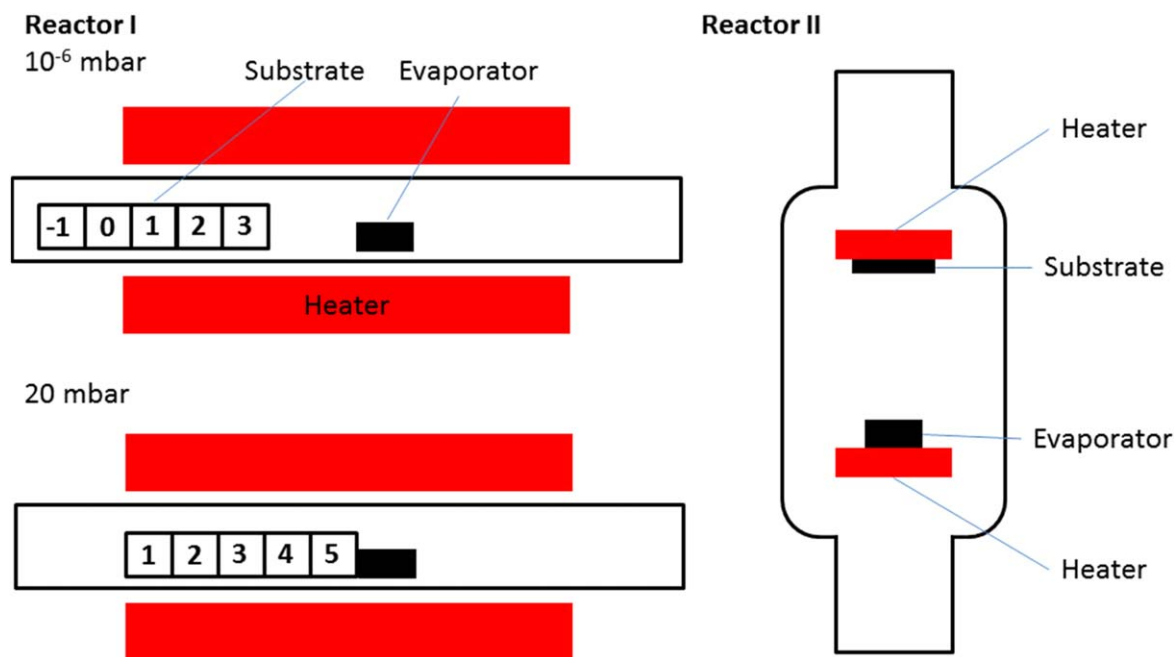
Figure 1. Schematic representation of **reactor** I (hot-wall reactor) and **reactor II** (cold-wall reactor). Note the different substrate position in **reactor I** depending on the reactor pressure.

furnace was cooled to ambient temperature within 30 min under vacuum.

X-ray analysis. XRD patterns were obtained using a Bruker D8 Advance powder diffractometer with Cu Kα radiation ($\lambda = 1.5418$ Å).

X-ray photoelectron spectroscopy. XPS studies were performed using a Versaprobe II™ (UlvacPhi) with mono-chromatic Al Kα light at 1486.6 eV photon energy. For depth-profiling this machine is equipped with an Ar-sputter source. The emission angle between analyzer and sample is 45°.

HRTEM analysis. TEM lamellas have been prepared using a Nova Nanolab 600 (FEI) Focused Ion Beam system. Most FIB preparation steps have been done at 30 kV accel-eration voltage. Due to the high beam sensitivity of the van der Waals bonded Sb$_2$Te$_3$ films, the last thinning steps were performed at 5 kV, only. This gives thin TEM lamellas with minimized surface damage and suitable for HRTEM. The HRTEM studies were performed using an image C_S corrected Titan 80-300 (FEI), lateral resolution limit 0.85 Å, at 300 kV acceleration voltage.

Transport measurements. The Hall coefficient was measured in magnetic fields ranging between –2 T and 2 T, in a temperature range of 7.5 to 300 K, using a closed cycle cryostat. The carrier concentration n was calculated by $n = 1/e \cdot R_\mathrm{H}$, where R_H is the Hall coefficient. The Con-ductivity σ was measured in 4-point geometry. The carrier mobility μ was calculated by $\mu = \sigma \cdot R_\mathrm{H}$. The Seebeck coefficient from 240 to 420 K was measured on a Linseis LSR-3 system. The Seebeck coefficient in cross-plane geo-metry was characterized using a potential Seebeck microp-robe from Panco GmbH.

3. Results and discussion

Reactor I. Commercial Sb$_2$Te$_3$ powder was evaporated in the center of a quartz tube placed in a horizontal tube furnace. The reactor temperature was varied from $T_\mathrm{evap} = 500\,^\circ$C–600 $^\circ$C, while the reactor pressure was kept constant at $5 \cdot 10^{-6}$ mbar. Si(100) substrates (50 mm · 10 mm) were divided into 10 mm by 10 mm sections (figure 1). Due to the temperature gradient between the heating zone and the outlet of the furnace, the substrate temperature ranged from 70 $^\circ$C (section −1) to 225 $^\circ$C (section 3). The evaporation rate of Sb$_2$Te$_3$ was found to be strongly dependent of the reactor temperature. Figure 2 shows the SEM photographs of different substrate sections of a material film that was deposited at $T_\mathrm{evap} = 600\,^\circ$C (these photographs are displayed in larger size in the electronic supplement, which is available online at stacks.iop.org/SST/ 33/105002/mmedia). Sections at low substrate temperatures T_Sub (sections −1, 0) show a rough surface morphology consisting of 500 nm thick hexagons. These structures consist of stacks of thinner hexagons that grew tilted on the substrate surface. The hexagon stacks become thinner and more defined at moderate substrate temperatures (sections 1, 2). In contrast, films grown at higher substrate temperatures (section 3) consist of hexagons that are preferentially grown *c*-oriented on the substrate.

The EDX analysis of the as-deposited Sb$_2$Te$_3$ films (table 1) shows a strong influence of the evaporation temp-erature T_evap, but only a weak influence of the substrate temperature. At high T_evap (550 $^\circ$C, 600 $^\circ$C), the Sb$_2$Te$_3$ powder was completely evaporated and the film composition was found to be Te-deficient. At a lower T_evap of 500 $^\circ$C, only
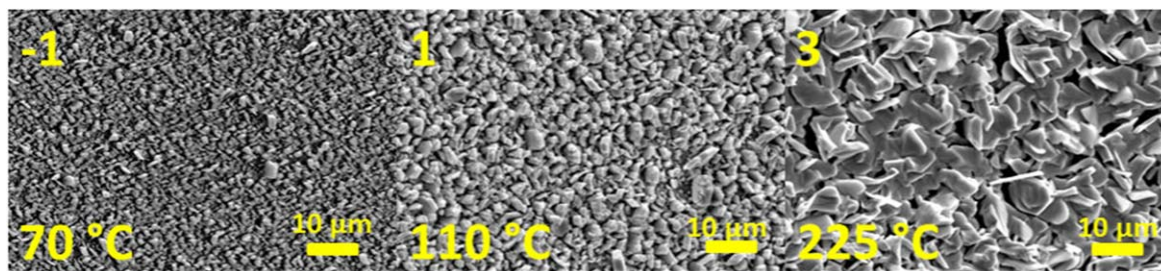
Figure 2. SEM photographs of different sections of material films grown on Si(100) substrates at $T_{evap} = 600\,^{\circ}C$ in **reactor I** at $5 \cdot 10^{-6}$ mbar.
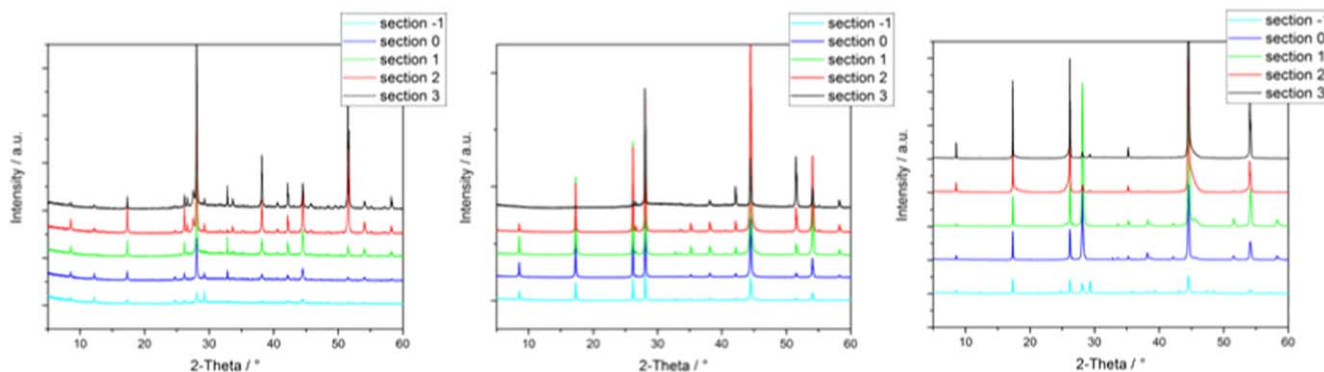

Figure 3. X-ray diffractograms of Sb_2Te_3 films grown on Si(100) (sections $-1 \ldots 3$) at $T_{evap} = 500\,^{\circ}C$ (left), $550\,^{\circ}C$ (middle) and $600\,^{\circ}C$ (right); **reactor I**, $5 \cdot 10^{-6}$ mbar.

Table 1. Sb:Te [at-%] molar ratio of Sb_2Te_3 films grown on Si(100) (section -1 to 3) at $T_{evap} = 500, 550$ and $600\,^{\circ}C$ in **reactor I** at $5 \cdot 10^{-6}$ mbar as determined by EDX analysis.

$T_{evap.}$ [$^{\circ}$C]	Section -1	Section 0	Section 1	Section 3	Section 3
600	46.9 : 53.1	46.3 : 53.7	46.4 : 53.6	46.3 : 53.7	43.1 : 56.9
550	38.7 : 61.3	38.8 : 61.2	38.7 : 61.7	38.7 : 61.3	38.6 : 61.4
500	41.2 : 58.8	40.1 : 59.9	39.4 : 60.6	40.2 : 59.8	41.2 : 58.8

40 mg of the Sb_2Te_3 powder was evaporated, but a film with a nearly stoichiometric Sb to Te ratio of 2:3 was obtained.

The XRD patterns for the Sb_2Te_3 film grown on sections -1 to 3 at different T_{evap} are displayed in figure 3. For all samples, the presence of rhombohedral Sb_2Te_3 was confirmed by comparison with the reported peak positions (PDF 15-874). The film deposited at $T_{evap} = 500\,^{\circ}C$ contained small amounts of elemental Te (PDF 36-1452) as secondary phase as determined by XRD. In general, the films were strongly textured and became more *c*-oriented with increasing T_{evap} and T_{sub}. The intensity ratio between the 006 reflection at $2\Theta = 26.3^{\circ}$ and the 015 reflection $2\Theta = 28.3^{\circ}$ was used to estimate the degree of *c*-orientation. At $T_{evap} = 600\,^{\circ}C$, the 015 reflection was almost fully suppressed and the reflections corresponding to the 00l crystal planes (l = 3, 6, 9, 12 …) were strongly pronounced, indicating a high degree of *c*-orientation.

The growth of Sb_2Te_3 films was then investigated at a working pressure of 20 mbar and the Sb_2Te_3 powder was evaporated at $600\,^{\circ}C$. The change of the pressure conditions from $5 \cdot 10^{-6}$ mbar to 20 mbar not only shifted the growth zone of the Sb_2Te_3 films towards higher substrate temperatures compared to the experiments at $5 \cdot 10^{-6}$ mbar, but also resulted in the growth of several micrometer large Te crystals in addition to very thin Sb_2Te_3 plates on the cold end of the subtrate (sections 1, 2). In contrast, pure Sb_2Te_3 plates were grown at higher substrate temperatures (section 3). The thickness of the Sb_2Te_3 plates increased with increasing substrate temperature, finally resulting in thin films at $370\,^{\circ}C$ (section 5) as shown in figure 4. The Sb_2Te_3 plates grew highly *c*-oriented with respect to the substrate surface, but very few freestanding discs were present. The elemental composition of the Sb_2Te_3 flakes were determined by EDX analysis. Regardless of the substrate position, Sb:Te ratios close to the ideal composition of 40:60 at% were found.

To investigate the influence of the substrate material on the morphology and chemical composition of the resulting Sb_2Te_3 films, we further investigated the growth on $Al_2O_3(0001)$ substrates. SEM photographs (figure 5) of the resulting films reveal the growth of exclusively *c*-oriented Sb_2Te_3 flakes on the substrate, which already starts at moderate substrate temperatures (section 3), whereas vertical and agglomerated discs are formed at lower substrate temperatures (sections 1, 2). With increasing substrate temperature,
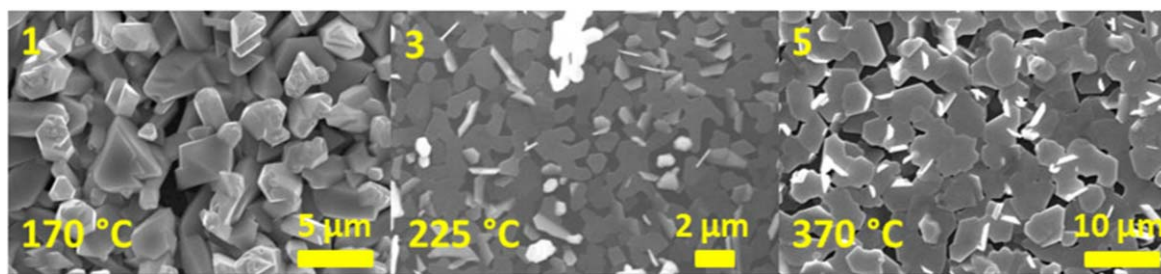
Figure 4. SEM photographs of Sb$_2$Te$_3$ films grown on Si(100) substrates at different substrate sections (**reactor I**, 20 mbar).
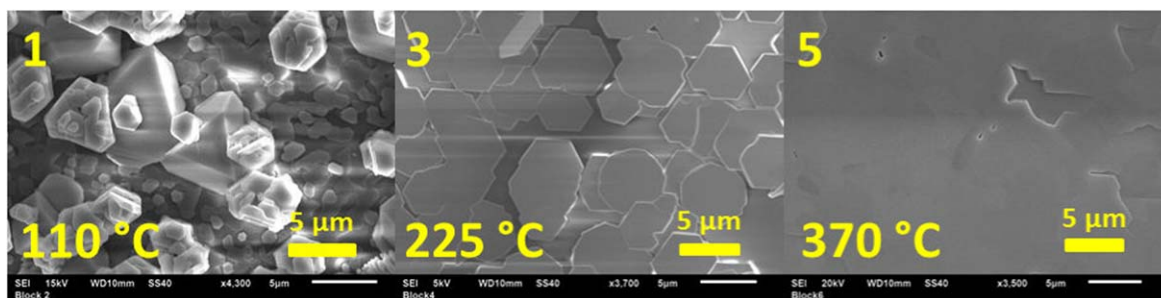

Figure 5. SEM photographs of Sb$_2$Te$_3$ films grown on Al$_2$O$_3$(0001) substrates at different substrates temperatures (**reactor I**, 20 mbar).
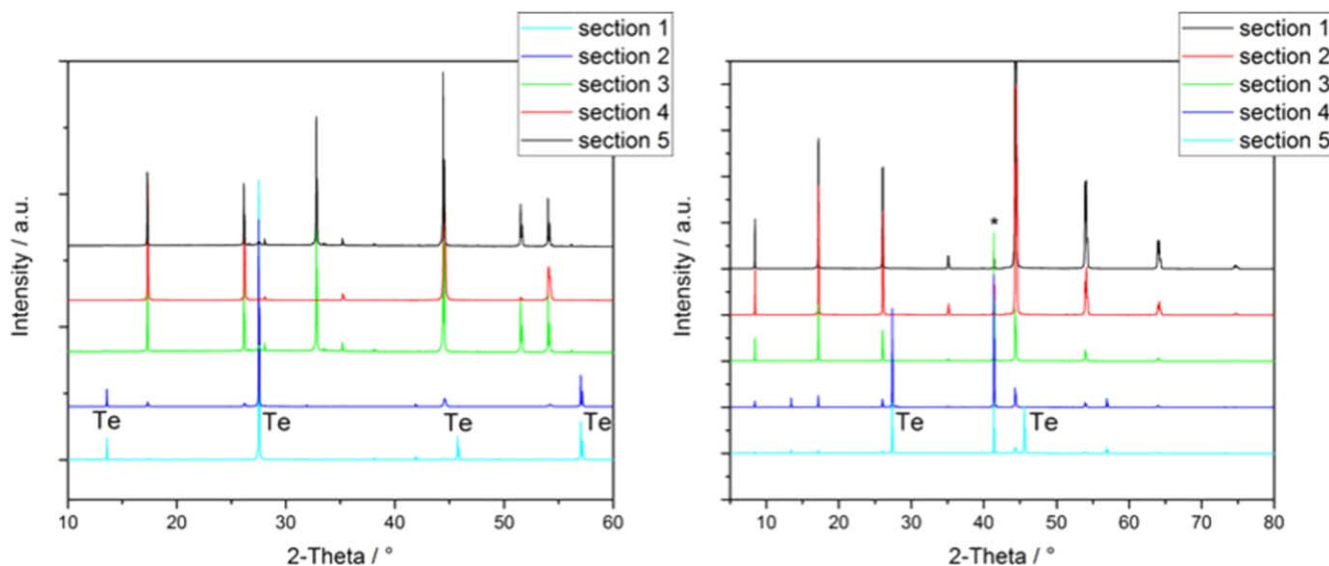

Figure 6. X-ray diffractogram of Sb$_2$Te$_3$ films grown on Si(100) (left) and Al$_2$O$_3$(0001) (right) substrates on different substrate sections in **reactor I** at 20 mbar.

the flakes were found to coalesce into closed and smooth Sb$_2$Te$_3$ films (sections 4, 5). The EDX analysis of as-formed films proved the formation of stoichiometric Sb$_2$Te$_3$ films on sections 3–5.

The growth of highly *c*-oriented Sb$_2$Te$_3$ films is supported by the XRD analysis (figure 6). Starting with section 3, only reflections corresponding to the 00l (l = 3, 6, 9, 12 …) lattice planes of phase-pure Sb$_2$Te$_3$ were observed. The presence of any additional second crystalline phase, including Sb, Sb$_2$O$_3$, Te and TeO$_2$, can be excluded.

The deposition experiments on Si(100) substrates in **reactor I** showed that the reactor pressure plays an important role in the deposition of high quality Sb$_2$Te$_3$ films. The films

grown at low pressure conditions (5 · 10^{-6} mbar) are dense and do not show any tendency towards the formation of holes, but rather show rough surface morphologies. In contrast, high pressure conditions (20 mbar) resulted in high deposition rates, but the as-formed films are non-stoichiometric and contain secondary phases of elemental Sb and/or Te. In addition, increasing the reactor pressure from 5 · 10^{-6} mbar to 20 mbar shifted the growth zone towards higher substrate temperatures. The resulting Sb$_2$Te$_3$ films show a strong *c*-orientation and exhibit a nearly stoichiometric chemical composition (Sb:Te molar ratio of 2:3). Clearly, the evaporation of Te from the as-deposited film is suppressed under these high-pressure conditions (20 mbar). Moreover, the
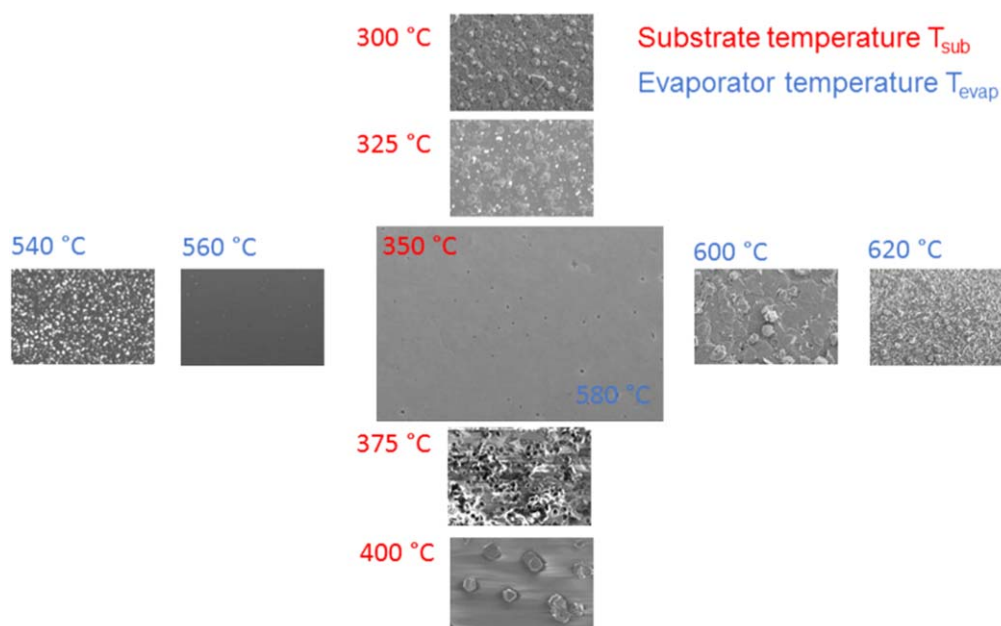
Figure 7. SEM photographs of Sb_2Te_3 films grown on $Al_2O_3(0001)$ substrates at different substrate and evaporator temperatures grown in **reactor II** at 20 mbar.

substrate material also plays a vital role in the growth of high-quality epitaxial Sb_2Te_3 films. While highly textured Sb_2Te_3 films were grown on Si(100), most likely due to the presence of a thin (amorphous) silicon oxide layer, epitaxial Sb_2Te_3 films were obtained on c-$Al_2O_3(0001)$ (c-Al_2O_3) substrates instead. In contrast, PVD growth experiments of Sb_2Te_3 films on Al_2O_3 substrates with different orientation (11–20 (A) and 1–100 (M)) did not yield epitaxial films (see electronic supplement).

To investigate the growth of high-quality Sb_2Te_3 films in more detail and to gain a better control over the growth conditions, we modified the reactor geometry. In this case, a cold-wall reactor with independently heated sample and substrate holders was developed to favor the growth of large and homogeneous Sb_2Te_3 films.

Reactor II. A cold-wall reactor for the deposition of smooth epitaxial Sb_2Te_3 films on $Al_2O_3(0001)$ substrates was developed (figure 1). Its design was based on the initial experiments in the horizontal tube reactor. In contrast to the tube reactor, the use of independent heaters for the substrate and the evaporator allows for a more precise control over the deposition conditions such as the substrate and evaporation temperatures, as well as the resulting growth rate. Optimal conditions for the deposition of Sb_2Te_3 films were found by systematic variations of the substrate and the evaporator temperatures. All experiments were performed at a reactor pressure of 20 mbar. The evaporator temperature in the first deposition series was fixed to 580 °C and the substrate temperature was varied between 300 °C and 400 °C. Dense films were grown at 300 °C, which showed a rather rough surface morphology due to the formation of isolated Sb_2Te_3 columns. Increasing the substrate temperature to 325 °C resulted in the reduction of columnar structures, while a further increase of the substrate temperature to 350 °C resulted in
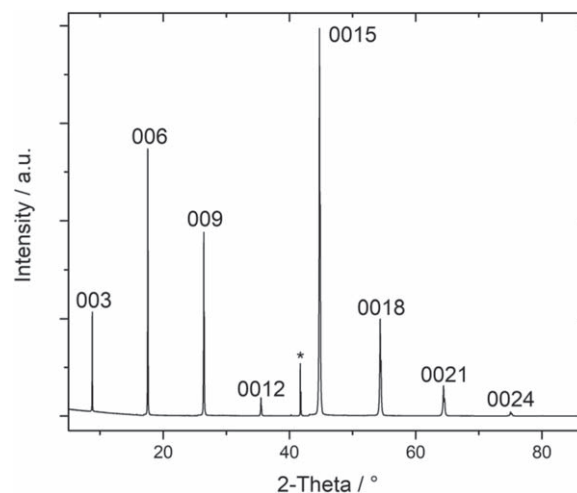

Figure 8. X-ray diffractogram of a Sb_2Te_3 film grown at 350 °C on a $Al_2O_3(0001)$ substrate grown in **reactor II**.

the growth of very smooth and continuous Sb_2Te_3 films. In contrast, substrate temperatures of 375 and 400 °C resulted in the growth of isolated hexagons instead of continuous Sb_2Te_3 films, likely due to higher desorption rates from the substrate surface (figure 7).

In a second deposition series, the substrate temperature was fixed to 350 °C and the evaporator temperature was varied between 540 to 620 °C. At a low evaporator temperature of 540 °C, the deposited film exhibited several holes. This behavior strongly indicates an insufficient supply of material flux. Dense and smooth films were obtained at 560 and 580 °C, whereas rough films were obtained at higher temperatures due to a higher precursor flux reaching the substrate.

The XRD pattern of a Sb_2Te_3 film grown at 350 °C on an $Al_2O_3(0001)$ substrate in reactor **II** is shown in figure 8. All
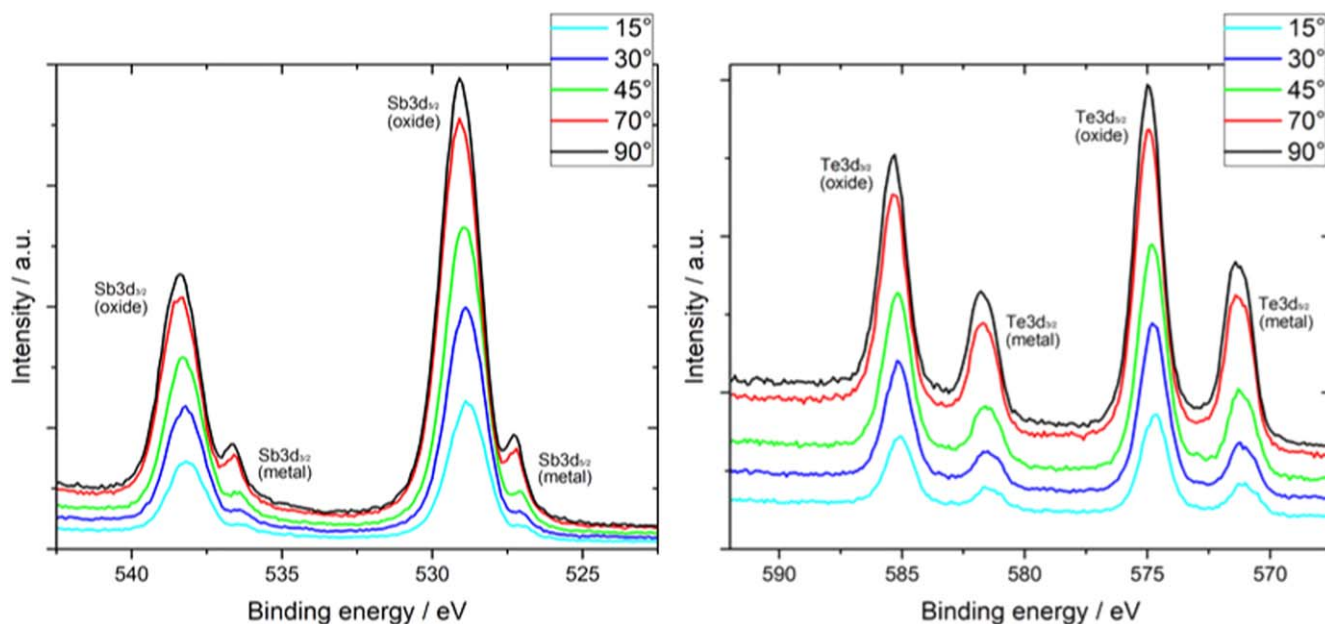
Figure 9. XPS core level Sb (left) and Te (right) spectra of a Sb_2Te_3 film grown at 350 °C on a Al_2O_3(0001) substrate.
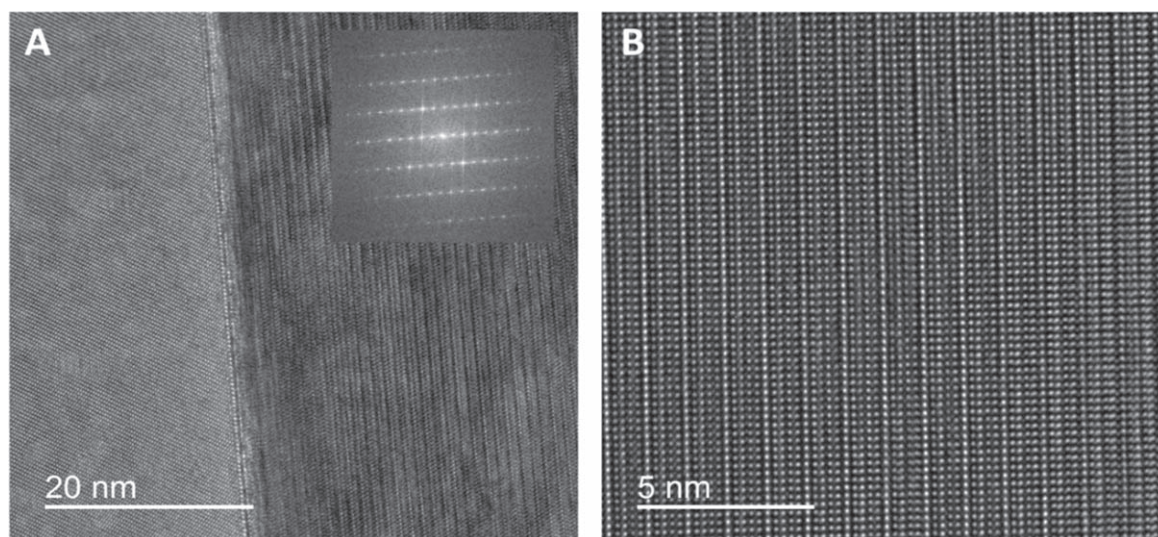

Figure 10. HRTEM image of the substrate film interface of a 500 nm thick Sb_2Te_3 film including a FFT of the film as inset, showing 001 growth (A). HRTEM image of a sectioned area in a 200 nm thick Sb_2Te_3 film with higher magnification, revealing high crystallinity and highly regular growth (B). Both films are grown at 333 °C on Al_2O_3(0001) substrates.

Bragg reflections with a significant intensity can be indexed on the basis of the structure of rhombohedral Sb_2Te_3. There is no indication for the formation of elemental Sb or Te as well as the corresponding oxides (Sb_2O_3, TeO_2). The XRD pattern shows the characteristic $00l$ ($l = 3, 6, 9, 12 …$) reflections for c-orientated Sb_2Te_3 (PDF 15-874).

The x-ray photoelectron spectrum (XPS) of a Sb_2Te_3 film grown on an Al_2O_3(0001) substrate at 350 °C (figure 9) shows strong peaks for Sb $3d_{3/2}$ and $3d_{5/2}$ at 539 and 529 eV and Te $3d_{3/2}$ and $3d_{5/2}$ at 582.9 and 572.5 eV, respectively. These values are in good agreement with reported binding energies of Sb and Te oxide species, indicating that the film surface is covered with a thin layer of $Sb_2Te_{3-x}O_x$ that is either amorphous or too thin to be detected by XRD. In addition, a second set of weak peaks at lower binding energies is visible for the elements corresponding to metallic antimony and tellurium in Sb_2Te_3. An angle-dependent measurement was used to calculate the thickness of the oxidized surface layer. The XPS study shows a partially oxidized surface of 3.2 ± 1.1 nm thickness [22].

A TEM lamella of a Sb_2Te_3 film was prepared by the focused ion beam technique to investigate the film-substrate interface by HRTEM in more details. The FFT pattern is shown as inset in figure 10(A). The growth of the Sb_2Te_3 film starts with one or two quintuple layers, which are rather largely disordered according to the HRTEM study. The disorder at the interface between the Al_2O_3 substrate and the growing Sb_2Te_3 film most likely results from the partial oxidation of
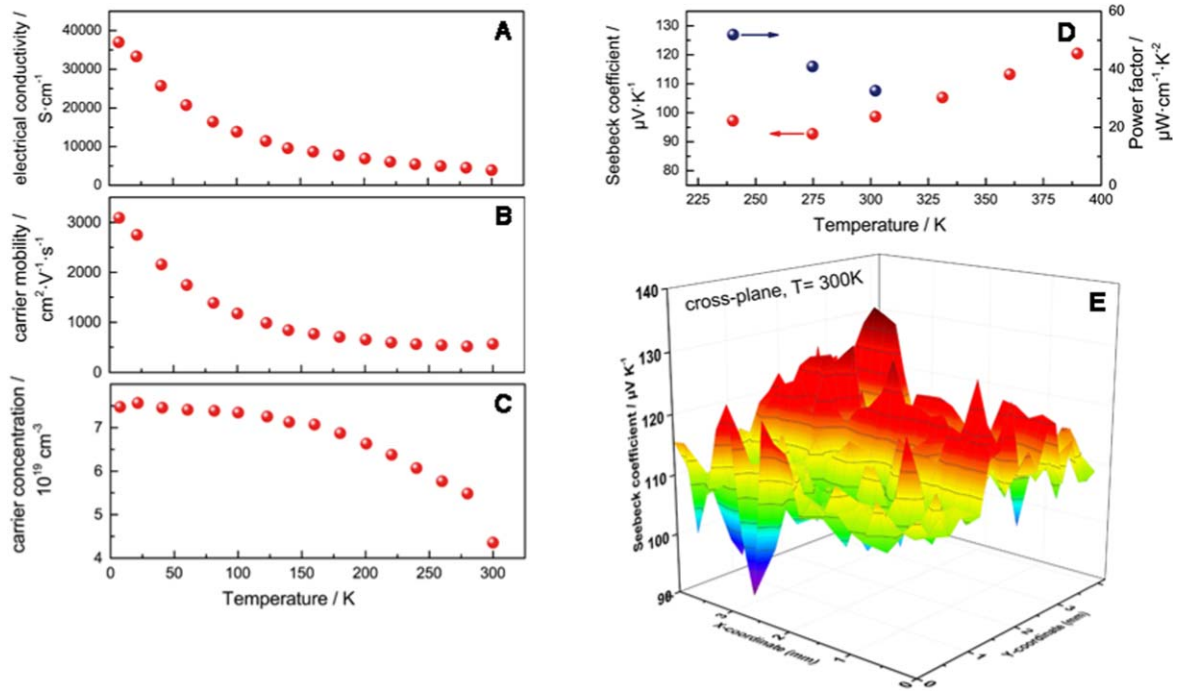
Figure 11. Electrical conductivity, carrier concentration, carrier mobility and Seebeck coefficient of a Sb_2Te_3 film grown at 350 °C on a $Al_2O_3(0001)$ substrate as a function of the temperature.

Table 2. Comparison of the thermoelectric and transport properties of the Sb_2Te_3 film at 300 K with other references.

Growth methode	n 10^{-19} cm^{-3}	σ S · cm^{-1}	μ cm^2 · V^{-1} · s^{-1}	S μV · K^{-1}	PF μW · cm^{-1} · K^{-2}	References
Thermal evaporation	4.3	3950	558	97	33	This work
MBE	2.6	1696	402	130	29	[25]
ALD	0.24	104	270.5	146.0	22.1	[27]
Co-evaporation	1.4	775	303	160	20	[20]
Bridgman (single crystal)	8.1	4762	365	79	30	[24]

the first Sb_2Te_3 layers [23]. Thereafter, highly crystalline quintuple layers of Sb_2Te_3 are epitaxially grown, and show very low number of stacking faults.

The temperature dependence of *in-plane* transport properties such as the carrier concentration n, the carrier mobility μ, and the conductivity σ of epitaxial Sb_2Te_3 films grown at 350 °C on $Al_2O_3(0001)$ was determined by a combined conductivity and Hall effect measurement. In figure 11(A), the electrical conductivity of the Sb_2Te_3 film as a function of the temperature is displayed. The film shows a metallic behavior and a monotonic decrease of the electrical conductivity with increasing temperature as was previously observed for MOCVD-grown epitaxial Sb_2Te_3 thin films [10]. At 300 K an electrical conductivity of 3950 S · cm^{-1} was measured. The film showed a high p-type carrier concentration (figure 11(C)) of $7.5 \cdot 10^{-19}$ cm^{-3} which remained nearly constant for temperatures T < 100 K, and then decreases with increasing temperature to $4.3 \cdot 10^{-19}$ cm^{-3} at 300 K. In consistence with the observed metallic behavior, the carrier mobility (figure 11(B)) decreases with increasing temperature reaching 558 cm^2 · V^{-1} · s^{-1} at 300 K. Remarkably, the carrier mobility is even higher than the value

reported for single crystals (365 cm^2·V^{-1} · s^{-1}) [24]. Comparable high values are only found for epitaxial or highly textured Sb_2Te_3 films (table 2). For example, a carrier mobility of 330 cm^2 · V^{-1} · s^{-1} was reported for MOCVD grown films [22], 303 cm^2 · V^{-1} · s^{-1} for thermal co-evaporated films [20], and 433 cm^2 · V^{-1} · s^{-1} for Sb_2Te_3 films prepared by nano-alloying [25], whereas lower values were reported for polycrystalline Sb_2Te_3 samples prepared by thermal evaporation in high vacuum [26]. figure 11(D) shows the Seebeck coefficient and the power factor values of a Sb_2Te_3 film with respect to temperature (240–420 K). The Seebeck coefficient monotonically increases in the temperature region from 94 μV · K^{-1} at 270 K to 127 μV · K^{-1} at 420 K. Based on the electrical conductivity and the Seebeck coefficient, a power factor of 33 μW·cm^{-1} · K^{-2} was calculated. The cross-plane Seebeck characterization at room temperature (figure 11(E)) showed good overall homogeneity and a Seebeck coefficient of 113 μV +−6 μV in the scanned area of 4 mm × 4 mm. We recently reported on *cross-plane* measurements of the thermal conductivity of epitaxial Sb_2Te_3 films using the 3-omega method. At 300 K, a very low

thermal conductivity of 1.6 $W \cdot m^{-1} \cdot K^{-1}$ was observed [23].

4. Conclusion

Sb_2Te_3 films were grown on Si(100) and Al_2O_3(0001) substrates by thermal evaporation of Sb_2Te_3 powders. Two different reactors were used and the deposition conditions (pressure, evaporator and substrate temperatures, substrate material) were systematically varied. Sb_2Te_3 films with rough surface topology were obtained on Si(100) substrates at low working pressure ($5 \cdot 10^{-6}$ mbar) in a horizontal hot-wall reactor, whereas higher working pressure (20 mbar) shifted the growth zone to higher substrate temperatures and allowed the growth of highly *c*-oriented Sb_2Te_3 films on Si(100) substrates. Epitaxial film growth was finally realized on Al_2O_3(0001) substrates at higher substrate temperatures (350 °C) and similar conditions.

The deposition process was further optimized using a cold-wall reactor with independent heaters for the substrate and the evaporator cell. Highly stoichiometric, epitaxial Sb_2Te_3 films with low surface roughness were again grown on rather large substrate areas at a substrate temperature of 350 °C and a working pressure of 20 mbar. HRTEM investigations revealed the growth of crystalline epitaxial Sb_2Te_3 films with very low lattice defect concentrations. The *in-plane* transport properties of as-formed Sb_2Te_3 films were measured; a high carrier mobility of $558 \, cm^2 \cdot V^{-1} \cdot s^{-1}$ and a moderate Seebeck coefficient of $97 \, \mu V \cdot K^{-1}$ a 300 K were observed. Based on the electrical conductivity and the Seebeck coefficient, a power factor of $33 \, \mu W \cdot cm^{-1} \cdot K^{-2}$ was calculated.

ORCID iDs

Stephan Schulz ⓘ https://orcid.org/0000-0003-2896-4488

References

[1] Haken W 1910 *Ann. Phys.* **337** 291

[2] Scherrer H and Scherrer S 1995 ed D M Rowe *CRC Handbook of Thermoelectrics* (New York: CRC Press) p 211

[3] Politano A, Viti L and Vitiello M S 2017 *APL Materials* **5** 035504

[4] Gooth J, Schierning G, Felser C and Nielsch K 2018 *MRS Bull.* **43** 187

[5] Moore J E 2010 *Nature* **464** 194

[6] Zhang J, Chang C Z, Zhang Z, Wen J, Feng X, Li K, Liu M, He K, Wang L A and Chen X *Nat. Commun.* **2** 574

[7] Heremans J P, Cava R J and Samarth N 2012 *Nat. Rev. Mater.* **2** 49

[8] Wang L L and Johnson D D 2011 *Phys. Rev. B—Condens. Matter Mater. Phys.* **83** 1

[9] Cao H, Venkatasubramanian R, Liu C, Pierce J, Yang H, Zahid Hasan M, Wu Y and Chen Y P 2012 *Appl. Phys. Lett.* **101** 162104

[10] Bendt G, Zastrow S, Nielsch K, Mandal P S, Sánchez-Barriga J, Rader O and Schulz S 2014 *J. Mater. Chem. A* **2** 8215

[11] He L, Kou X and Wang K L 2013 *Phys. Status Solidi—Rapid Res. Lett.* **7** 50

[12] Takashiri M, Tanaka S and Miyazaki K 2014 *J. Electron. Mater.* **43** 1881

[13] Völklein F, Baier V, Dillner U and Kessler E 1990 *Thin Solid Films* **187** 253

[14] Takashiri M, Tanaka S and Miyazaki K 2010 *Thin Solid Films* **519** 619

[15] Takashiri M, Tanaka S, Hagino H and Miyazaki K 2014 *Int. J. Heat Mass Transf.* **76** 376

[16] Goncalves L M, Alpuim P, Rolo A G and Correia J H 2011 *Thin Solid Films* **519** 4153

[17] Goncalves L M, Alpuim P, Min G, Rowe D M, Couto C and Correia J H 2008 *Vacuum* **82** 1499

[18] Lin J M, Chen Y C, Yang C F and Chen W 2015 *Journal of Nanomaterials* **2015** 135130

[19] Lin J M, Chen Y C and Chen W 2015 *Journal of Nanomaterials* **2015** 564954

[20] Zou H, Rowe D M and Williams S G K 2002 *Thin Solid Films* **408** 270

[21] Huang B, Lawrence C, Gross A, Hwang G S, Ghafour N, Lee S W, Kim H, Li C P, Uher C and Najafi C 2008 *J. Appl. Phys.* **104** 113710

[22] Bendt G, Sonntag J, Lorke A, Assenmacher W, Hagemann U and Schulz S 2015 *Semicond. Sci. Technol.* **30** 85021

[23] Rieger F, Kaiser K, Bendt G, Roddatis V, Thiessen P, Schulz S and Jooss C 2018 *J. Appl. Phys.* **125** 175108

[24] Stordeur M, Stölzer M, Sobotta H and Riede V 1988 *Phys. Status Solidi* B **150** 165

[25] Peranio N, Winkler M, Bessas D, Aabdin Z, König J, Böttner H, Hermann R P and Eibl O 2012 *J. Alloy. Compd.* **521** 163

[26] Aboulfarah B, Sayah D, Mzerd A, Giani A and Boyer A 2000 *M. J. Condens. Matter* **3** 76

[27] Zastrow S, Gooth J, Boehnert T, Heiderich S, Toellner W, Heimann S, Schulz S and Nielsch K 2013 *Semicond. Sci. Technol.* **28** 035010